COMMUNICATION

CrossMark
click for updates

Ultrasmall cobalt nanoparticles supported on nitrogen-doped porous carbon nanowires for hydrogen evolution from ammonia borane†

Limin Zhou,[ab] Jing Meng,[a] Pan Li,[a] Zhanliang Tao,*[a] Liqiang Mai[b] and Jun Chen[a]

Design and fabrication of stable and coordinated composite nano-architectures seem particularly essential for enhancing the catalytic activity and reusability of catalysts. Herein, we report the preparation of cobalt nanoparticles supported on nitrogen-doped porous carbon nanowires (Co/NPCNW) and their remarkable catalytic activity for the hydrolysis of ammonia borane (AB).

Ammonia borane (NH_3BH_3, AB) is believed to be an attractive hydrogen carrier because of its high hydrogen capacity[1–5] and excellent stability in aqueous solutions at room temperature.[6–9] However, the sluggish kinetics of the AB hydrolysis reaction seriously impedes the hydrogen production efficiency. Therefore, searching for a suitable and efficient catalyst to improve the hydrogen evolution rate is indispensable. Currently, although noble-metal catalysts[10–14] are acknowledged to be a decent option due to their superior catalytic properties for AB hydrolysis, their practical application is severely restricted on account of high cost and limited available quantity. Thus, numerous efforts have been devoted to exploiting cheap and highly efficient Co-based catalysts.[15–18]

Previous reports have proved that the nano-size of materials is an utilizable approach to promote catalytic activity through the incorporation of surfactants or supports.[19–21] For instance, 8 nm CoPd nanoparticles have been synthesized by liquid-phase reduction with the help of oleylamine and trioctylphosphine, presenting an activation energy of 27.5 kJ mol^{-1}.[22] Subsequently, a polyethylenimine (PEI)-GO/Co composite was prepared by *in situ* deposition of metal nanoparticles on the PEI-GO surface, exhibiting 65.6% of the initial catalytic activity after the 5th cycle.[23] Cheng's group synthesized graphene supported Ru@Co core–shell

[a] Key Laboratory of Advanced Energy Materials Chemistry (Ministry of Education), Collaborative Innovation Center of Chemical Science and Engineering, College of Chemistry, Nankai University, Tianjin 300071, China. E-mail: taozhl@nankai.edu.cn

[b] State Key Laboratory of Advanced Technology for Materials Synthesis and Processing, Wuhan University of Technology, Hubei, Wuhan 430070, China

Conceptual insights

Searching for a suitable and efficient catalyst to improve the hydrogen evolution rate from ammonia borane (AB) is urgent and indispensable. Current reports focus on the nano-size of particles by the introduction of surfactants and an external support to promote catalytic activity. However, the surfactants might form a coating on the active sites and hence lead to deteriorated catalytic activity and the external support may be unable to mitigate the agglomeration of nanoparticles. In this work, we demonstrate a facile *in situ* carbonization and reduction strategy to achieve a steady supporting stucture and nano-sized active sites. Our work has the following new contributions: (1) An MOF-driven approach was adopted to realize the nano-sized particles and nitrogen-doped supporting architecture without the introduction of a foreign material, favorable for increasing the catalytic active sites and effectively immobilizing the catalytic active materials. (2) The synergistic effect of the structure and morphology enables the material to demonstrate an outstanding catalytic performance (a hydrogen generation rate of 2638 mL min^{-1} g^{-1} and 94.6% maintenance of their initial catalytic activity after 10 runs). (3) Significantly, this approach could be extended to the preparation of other similar structural catalysts and could provide the basis for a N-doped steady porous catalyst for AB hydrolysis in hydrogen storage application.

nanoparticles *via in situ* co-reduction, demonstrating 51% of the initial catalytic activity in the 5th run.[24] Despite some enhancement of catalytic activity, the above methods are generally limited to the introduction of surfactants or supports, which couldn't essentially avoid the agglomeration and the loss of active materials.[18,25] Moreover, the surfactants might form a coating on the active sites and lead to deteriorated catalytic activity.[26]

To tackle these problems, carbonization of an inorganic–organic composite is a reasonable approach to realize efficient species,[27–31] including the desired favorable elements and uniformly dispersed catalytic sites and a tenable entire structure. Our group synthesized Sn nanoparticles embedded in porous N-doped carbon networks (5-Sn/C) by carbonizing divalent Sn(Salen),[27] which are used for the electrode material. The products consist of interconnected porous carbon frameworks and uniformly distributed small-scale nanoparticles.[27,32,33] Thus, the strategy is worthy of being attempted.

In this work, cobalt nanoparticles ($\sim$3.5 nm) finely supported on nitrogen-doped porous carbon nanowires (denoted as Co/NPCNW) were fabricated by direct carbonization of a Co-metal organic framework (Co-MOF) without the introduction of a foreign material. During the pyrolysis process, a cobalt cation is *in situ* reduced to ultrasmall nanoparticles and the ligand is converted to carbon networks, simultaneity, nitrogen contained in the ligand is converted to a variety of N species (pyridinic N, pyrrolic N, graphitic N). The resultant Co/NPCNW showed a high hydrogen generation rate (2638 mL min^{-1} g^{-1}), a relatively low activation energy (25.4 kJ mol^{-1}), and excellent reusability for AB hydrolysis.

The preparation of Co/NPCNW followed a two-step route. First, the solvothermal synthesis of the Co-MOF was carried out, in which Co(NO$_3$)$_2$·6H$_2$O acted as the metal salt, H$_3$BTC (H$_3$BTC = 1,3,5-benzenetricarboxylic acid) and 4,4′-bipy (4,4′-bipy = 4,4′-bipyridine) served as the organic ligand. The XRD pattern of the Co-MOF shown in Fig. S1 (ESI†) is consistent with the structure analysis reported in the literature[34] and the Co-MOF has a relatively large specific surface area of 862.7 m^2 g^{-1}

(ESI,† Fig. S2). Then, the Co-MOF was pyrolyzed at 700 °C for 2 h under an Ar atmosphere (as illustrated in Fig. 1a). The morphology of Co/NPCNW was characterized using scanning electron microscopy (SEM) and transmission electron microscopy (TEM), respectively. The porous nanowires decorated with uniform Co nanoparticles are several micrometers in length (Fig. 1b–d). These small nanoparticles are found to have a mean particle diameter of 3.5 nm (the inset of Fig. 1d). The high-resolution TEM (HRTEM) image of Co/NPCNW (Fig. 1e) presents highly dispersed cobalt nanoparticles, in which the *d*-spacing is measured to be 0.20, 0.17, and 0.13 nm, coinciding with the (111), (200), and (220) planes of Co nanoparticles. Furthermore, elemental mapping confirms the homogeneous distribution of Co, C, and N on the carbon matrix in the selected range (Fig. 1f).

The effects of the calcination temperature and time on the structure and morphology were investigated. The temperature was determined by the thermogravimetric (TG) curve of the Co-MOF (ESI,† Fig. S3), revealing the loss of free water and the
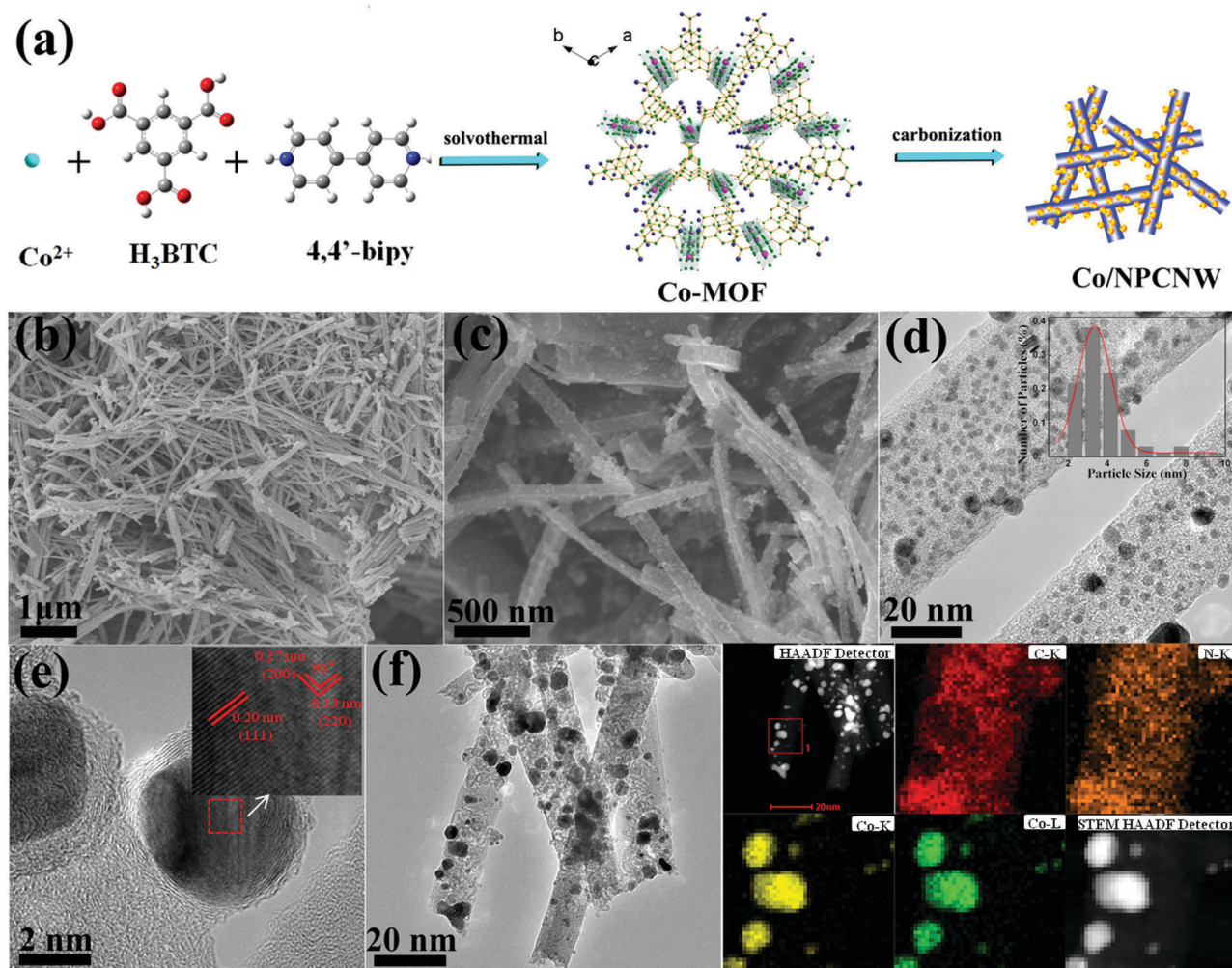

Fig. 1 (a) Conceptual schematic illustration of the synthetic route to Co/NPCNW. Morphology characterization: SEM (b and c), TEM (d), and high-resolution TEM (HRTEM) (e) images of Co/NPCNW, the inset of (d) is the corresponding size distribution of cobalt nanoparticles, the inset of (e) is the magnification of the rectangular region. (f) STEM (HAADF, Co, C, N) elemental mapping images of Co/NPCNW.
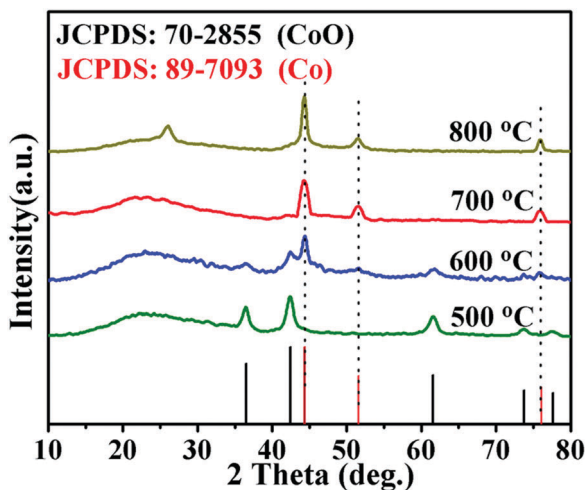
Fig. 2 XRD patterns of the as-prepared products of Co-MOF calcined at different calcination temperatures (500 °C, 600 °C, 700 °C, and 800 °C) for 2 h.

carbonization of the organic ligand along with the reduction of the metal cation before 500 °C. The products at different calcination temperatures (500 °C, 600 °C, 700 °C, and 800 °C) are denoted as Co-MOF-500, Co-MOF-600, Co-MOF-700, and Co-MOF-800, respectively. From the power X-ray diffraction (XRD) patterns (Fig. 2), it is found that Co-MOF-500 stands for a composite of CoO and amorphous carbon and Co-MOF-600 is a mixture of CoO, Co, and amorphous carbon.

However, both Co-MOF-700 and Co-MOF-800 display the peaks of metal cobalt and amorphous carbon, revealing complete conversion to carbonization and reduction products. The SEM images of Co-MOF-700 and Co-MOF-800 (ESI,† Fig. S4) illustrate that higher temperature results in the fracture and agglomeration of nanowires. Hence, the optimum calcination temperature appears to be 700 °C.

To further study the growth process of Co/NPCNW and explain the determination of the calcination time, the morphology of the Co-MOF and calcined products for different calcination times (1 h, 2 h, 3 h) at 700 °C is characterized by SEM (ESI,† Fig. S5). It can be seen that the surface of the Co-MOF is smooth. When calcined at 700 °C for 1 h, some dispersed nanoparticles appeared on the frameworks. When the calcination time is extended to 2 h, it is clearly observed that the porous carbon nanowires are peppered with dispersed nanoparticles. Concretely, the organic ligand is transformed to porous carbon frameworks and the metal cation is *in situ* reduced to active Co nanograins ($\sim$3.5 nm).[27,35] In addition, partial N species could be retained in the porous carbon networks, favorable for the hydrolysis performance.[36] Nevertheless, upon continuing to extend the calcination time to 3 h, the frameworks begin to fracture with the growth of particles. A comparison of the size distribution of cobalt nanoparticles calcined for 2 h and 3 h (ESI,† Fig. S6) strongly proves that the particles tend to agglomerate with the prolongation of the calcination time. The evolution process makes us come to the conclusion that the optimum calcination condition should be 700 °C for 2 h under an Ar environment.

The surface area and porosity of the as-synthesized Co/NPCNW are characterized by nitrogen adsorption–desorption isothermal analysis. The general shape of the N_2 sorption isotherms presented in Fig. 3a can be classified into type H4 according to the IUPAC nomenclature, which is characteristic of the appearance of a hysteresis loop at relative high pressure.[37] This kind of hysteresis loop is an echo of mesopores embedded in a matrix of the prepared carbon materials.[38] Besides, Co/NPCNW shows a relatively large specific surface area of 417.8 m^2 g^{-1} calculated by using the Brunanuer–Emmett–Teller (BET) equation, which is attributed to the porous structure of carbon nanowires and the uniform dispersity of ultrasmall Co particles. The Barrett–Joyner–Halenda (BJH) pore size distribution analysis of Co/NPCNW (the inset of Fig. 3a) reveals that the pore diameter of most pores is 5 nm, which coincides with the analysis of the hysteresis loop.

The element bonding configuration of Co/NPCNW is evaluated by X-ray photoelectron spectroscopy (XPS). Fig. 3b exhibits the high resolution XPS spectrum of Co 2p. The peak at around 778.6 eV is ascribed to zero-valent Co, confirming the appearance of cobalt nanoparticles during the calcination process, whereas the peak at 783.4 eV is consistent with the binding energy of cobalt oxide, perhaps due to the superficial oxidation of cobalt nanoparticles during the XPS sampling.[16] The C 1s XPS spectrum (Fig. 3c) shows three distinct peaks at 284.8 eV, 285.8 eV, and 288.6 eV, which can be well assigned to sp^2 C–sp^2 C, N–sp^2 C, and N–sp^3 C bonds, respectively.[28,39] The N 1s XPS spectrum (Fig. 3d) can be divided into several single peaks with binding energies at about 398.1 eV, 399.2 eV, 401.1 eV, and 402.8 eV, attributed to pyridinic N, pyrrolic N, graphitic N, and oxidized N successively,[40] which are believed to chemically tune the carbon matrix through diverse functional groups and enhance the structural defect of the carbon material.[41] It is worth noting that the existence of the N element thereby not only inherits the advantage of the homogeneous dispersion of cobalt nanoparticles,[42] but also heralds the enhancement of the chemical adsorptive force between carbon nanowires and cobalt nanoparticles through electron delocalization.[43] The concentration of extracted Co is 1.82 mg L^{-1} in the leaching test, further proving the integrity and stability of the *in situ* supported structure. A diagrammatic sketch of N-doped carbon nanowires is given in Fig. 3e. Besides, the ICP analysis reveals that the cobalt content in Co/NPCNW is approximately 51.6 wt%, which agrees with the calculated value 52 wt%, determined from the TG curve of Co/NPCNW (ESI,† Fig. S7).

Motivated by the desirable supported porous nanoarchitecture, the catalytic activity of Co/NPCNW was evaluated in the hydrolysis of AB and a series of kinetics experiments was carried out. First, the generated gas of AB hydrolysis was analyzed by gas chromatography (GC) for purity. The strong peak (ESI,† Fig. S8) confirms that the released H_2 is relatively pure and the quite weak peaks are ascribed to the unavoidable O_2 and N_2 from air. The results given in Fig. 4a show that the hydrolysis of AB went on at various temperatures in the range of 25–55 °C in the presence of 0.5 wt% AB and 10 mg Co/NPCNW catalyst. The equally spaced increase of temperature results in increasing hydrogen generation rate. From the plot of room temperature, we find that the turnover frequency (TOF) of the Co/NPCNW catalyst is 7.29 mol_{H_2} mol_{Co}^{-1} min^{-1}.
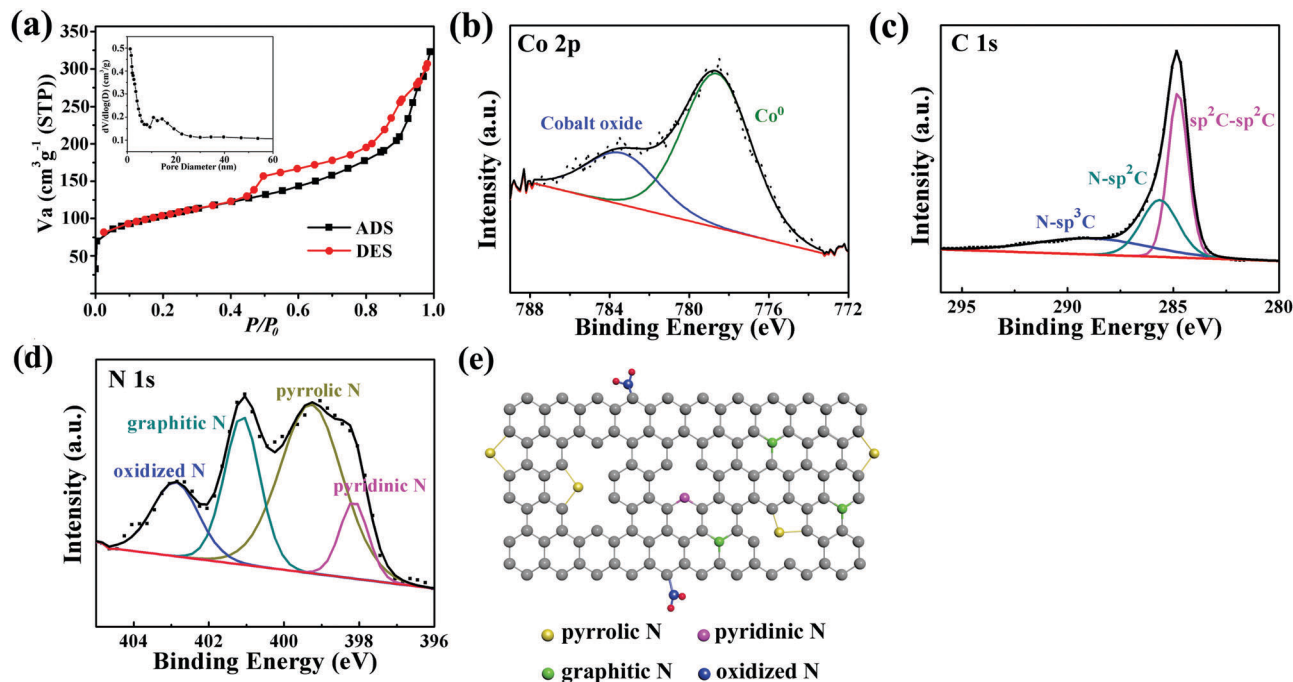
Fig. 3 Structure analysis. (a) N_2 adsorption–desorption isotherm of Co/NPCNW (the inset is the pore-size distribution of Co/NPCNW). High-resolution spectra of (b) Co 2p; (c) C 1s; (d) N 1s in the XPS spectrum of Co/NPCNW. (e) Representation of different types of N dopants present in Co/NPCNW based on XPS results.
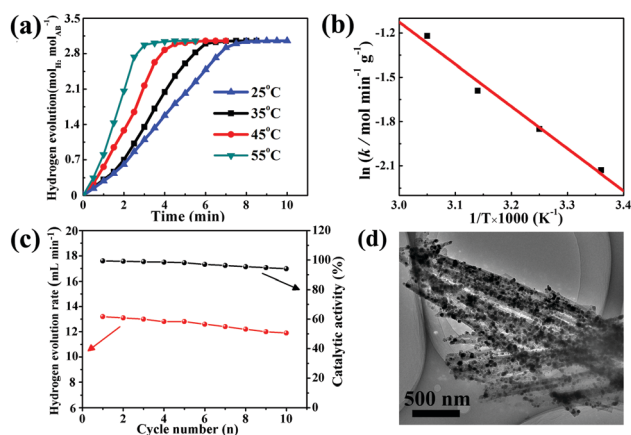

Fig. 4 Catalytic hydrolysis performance of Co/NPCNW. (a) Plot of equivalent H_2 per mole of AB vs. time generated from AB solution (0.5 wt%, 8 mL) using 10 mg Co/NPCNW in the temperature range of 25–55 °C, (b) the corresponding Arrhenius plots of ln k vs. absolute temperature 1/T. (c) The reusability and catalytic activity of Co/NPCNW for the hydrolysis of AB at different cycle numbers. (d) TEM image of Co/NPCNW as the catalyst for hydrolysis of AB after 10 cycles.

The Arrhenius plot of ln k vs. 1/T for the catalyst is given in Fig. 4b and the activation energy is calculated to be 25.4 kJ mol^{-1}. Upon careful examination, we can see that there is an induction period at the beginning in the hydrolysis reaction. Since the cobalt nanoparticles could easily be oxidized when exposed to air, the partially oxidized layer tends to be reduced first when AB powder is added, leading to the appearance of the induction stage similar to the behavior of other catalytic systems.[35] Zero-valent cobalt as an active catalyst is actually competent in the AB hydrolysis system compared

with the unavoidable superficial oxidized component. The induction stage during the hydrolysis of AB is just to reduce a small amount of the superficial oxidized layer, favorable for the successive hydrolysis reaction.

For the sake of exploring the acting mechanism of the N element during the hydrolysis process, Co nanoparticles supported on carbon nanorods (Co/C) were synthesized using the same procedure in the absence of 4,4′-bipyridine. The morphology of Co/C (ESI,† Fig. S9) demonstrated ultrasmall dispersed Co nanoparticles supported on carbon nanorods, like that of Co/NPCNW. Upon comparing the catalytic performance of Co/NPCNW and Co/C in the hydrolysis of AB (ESI,† Fig. S10), it is clearly observed that Co/NPCNW presents a better catalytic performance with a hydrogen evolution rate of 2638 mL min^{-1} g^{-1}. In addition, the IR spectra of AB, AB–Co/C and AB–Co/NPCNW (the mixtures of AB and Co/C (Co/NPCNW) are denoted as AB–Co/C (AB–Co/NPCNW)) are displayed (ESI,† Fig. S11). The wave number of the N–H bond from 3200 cm^{-1} to 3500 cm^{-1} for AB–Co/NPCNW shifts to a higher wave number compared with those of pure AB and AB–Co/C, indicating the enhancement of the N–H bond. The change in the wave number of the B–N bond can be clearly seen from the partially enlarged drawing (ESI,† Fig. S11b). The peaks of the B–N bonds in AB–Co/NPCNW clearly exhibit a red shift, confirming the attenuation of the B–N bond. Thus, N-doping is beneficial for the attenuation of the B–N bond, accelerating the rate-controlling step and lowering the activation energy of the reaction.

The plot of volume of H_2 versus time (ESI,† Fig. S12) was generated from AB hydrolysis catalyzed by a different amount of Co/NPCNW at room temperature (25 °C). From these curves,

we can see that the hydrolysis rate is dramatically enhanced with the increasing of the catalyst amount. The slope of the plot of ln rate *vs.* ln catalyst amount is 1.09, indicating that the hydrolysis of AB catalyzed by Co/NPCNW is a first-order reaction with respect to the catalyst concentration. In addition, the relationship between the TOF value and the amount of catalyst is shown in Fig. S13 (ESI†). When the amount of Co/NPCNW reaches an appropriate value in the AB hydrolysis system, the TOF stands for the property of the catalyst itself. The TOF of Co/NPCNW was 7.29 $mol_{H_2}\ mol_{Co}^{-1}\ min^{-1}$. The effect of AB concentration has also been studied (ESI,† Fig. S14). It is clearly recognized that the hydrolysis rate has no relationship with AB concentration and the slope of the ln rate *vs.* ln AB concentration plot is almost parallel to the transverse coordinates, which can be regarded as a zero-order reaction.

Considering the significance of an eco-friendly catalyst, the reusability of Co/NPCNW was investigated. In the reusability test, the catalysts were enabled to magnetically attach to the bottom of the flask. When the hydrolysis was completed, the supernatant liquid was removed and 40 mg AB powder was added to conduct the reusability test. From the catalytic activity of Co/NPCNW shown in Fig. 4c, it can be seen that 94.6% of the initial catalytic activity is retained even after 10 runs and the rate of hydrogen evolution is only slightly decreased. The TEM image of Co/NPCNW (Fig. 4d) after 10 cycles exhibits uniformly dispersed cobalt nanoparticles without the appearance of agglomeration and stripping. Subsequently, the reproducibility of Co/NPCNW was evaluated. A comparison of the XRD patterns of Co/NPCNW before and after 5 cycles (ESI,† Fig. S15) clearly demonstrates the preservation of the intrinsic phase of the catalyst. The TEM and HRTEM images of the catalyst after 5 cycles (ESI,† Fig. S16) further identify that the catalyst architecture is retained. The excellent catalytic performance can be attributed to the integration of the favorable structure and component. First, uniformly dispersed cobalt nanoparticles with a large surface area contribute to offer more catalytic active sites, favorable for the interaction between AB and the cobalt surface.[35,44,45] Second, the steady porous structure protects the Co active sites from agglomeration and provides more channels for the interaction between AB and the metal surface, conducive to the reusability of the Co/NPCNW and catalytic rate.[36] Third, the existence of the N element enables attenuation of the energy of the B–N bond, favorable for the rate-controlling step. All these are associated with the catalytic performance of Co/NPCNW compared with other Co-based catalysts (ESI,† Table S1).

In summary, we have synthesized cobalt nanoparticles supported on nitrogen-doped porous carbon nanowires (Co/NPCNW) by one-step carbonization of Co-MOF, which present a hydrogen generation rate of 2638 mL min^{-1} g^{-1} and a relatively low activation energy of 25.4 kJ mol^{-1}. Significantly, the preparation approach can directly achieve all the desired components (Co, C, N) and an ideal structure (well-distributed nanoparticles and a steadily supported porous construction), beneficial for the maintenance of the integrated structure and the improvement of the catalytic activity. The synergistic effect of the component and structure makes Co/NPCNW an outstanding catalyst for the hydrolysis of AB. This result should provide the basis for a N-doped steady porous catalyst for AB hydrolysis in hydrogen storage application.

Acknowledgements

Notes and references

1 A. Gutowska, L. Li, Y. Shin, C. M. Wang, X. S. Li, J. C. Linehan, R. S. Smith, B. D. Kay, B. Schmid and W. Shaw, *Angew. Chem., Int. Ed.*, 2005, **44**, 3578–3582.
2 T. B. Marder, *Angew. Chem., Int. Ed.*, 2007, **46**, 8116–8118.
3 X. Kang, Z. Fang, L. Kong, H. Cheng, X. Yao, G. Lu and P. Wang, *Adv. Mater.*, 2008, **20**, 2756–2759.
4 D. W. Himmelberger, C. W. Yoon, M. E. Bluhm, P. J. Carroll and L. G. Sneddon, *J. Am. Chem. Soc.*, 2009, **131**, 14101–14110.
5 G. Xia, X. Yu, Y. Guo, Z. Wu, C. Yang, H. Liu and S. Dou, *Chem. – Eur. J.*, 2010, **16**, 3763–3769.
6 J. M. Yan, X. B. Zhang, S. Han, H. Shioyama and Q. Xu, *Angew. Chem., Int. Ed.*, 2008, **120**, 2319–2321.
7 J. Zhao, J. Shi, X. Zhang, F. Cheng, J. Liang, Z. Tao and J. Chen, *Adv. Mater.*, 2010, **22**, 394–397.
8 C. Y. Peng, L. Kang, S. Cao, Y. Chen, Z. S. Lin and W. F. Fu, *Angew. Chem., Int. Ed.*, 2015, **54**, 15725–15729.
9 S. Rej, C.-F. Hsia, T.-Y. Chen, F.-C. Lin, J.-S. Huang and M. H. Huang, *Angew. Chem., Int. Ed.*, 2016, **55**, 7222–7226.
10 X. Yang, F. Cheng, J. Liang, Z. Tao and J. Chen, *Int. J. Hydrogen Energy*, 2009, **34**, 8785–8791.
11 H. L. Jiang, T. Umegaki, T. Akita, X. B. Zhang, M. Haruta and Q. Xu, *Chem. – Eur. J.*, 2010, **16**, 3132–3137.
12 N. Cao, W. Luo and G. Cheng, *Int. J. Hydrogen Energy*, 2013, **38**, 11964–11972.
13 Y. Z. Chen, Q. Xu, S. H. Yu and H. L. Jiang, *Small*, 2015, **11**, 71–76.
14 K. Mori, K. Miyawaki and H. Yamashita, *ACS Catal.*, 2016, **6**, 3128–3135.
15 U. B. Demirci and P. Miele, *Phys. Chem. Chem. Phys.*, 2014, **16**, 6872–6885.
16 H. Wang, Y. Zhao, F. Cheng, Z. Tao and J. Chen, *Catal. Sci. Technol.*, 2016, **6**, 3443–3448.
17 J. Li, Q.-L. Zhu and Q. Xu, *Catal. Sci. Technol.*, 2015, **5**, 525–530.
18 Q. Yao, Z.-H. Lu, Y. Hu and X. Chen, *RSC Adv.*, 2016, **6**, 89450–89456.
19 H.-L. Jiang, T. Akita and Q. Xu, *Chem. Commun.*, 2011, **47**, 10999–11001.
20 Y.-C. Luo, Y.-H. Liu, Y. Hung, X.-Y. Liu and C.-Y. Mou, *Int. J. Hydrogen Energy*, 2013, **38**, 7280–7290.
21 W. Chen, J. Ji, X. Feng, X. Duan, G. Qian, P. Li, X. Zhou, D. Chen and W. Yuan, *J. Am. Chem. Soc.*, 2014, **136**, 16736–16739.
22 D. Sun, V. Mazumder, O. Metin and S. Sun, *ACS Nano*, 2011, **5**, 6458–6464.
23 J. Hu, Z. Chen, M. Li, X. Zhou and H. Lu, *ACS Appl. Mater. Interfaces*, 2014, **6**, 13191–13200.

24 N. Cao, J. Su, W. Luo and G. Cheng, *Catal. Commun.*, 2014, **43**, 47–51.

25 L. Yang, N. Cao, C. Du, H. Dai, K. Hu, W. Luo and G. Cheng, *Mater. Lett.*, 2014, **115**, 113–116.

26 O. n. Metin, V. Mazumder, S. Ozkar and S. Sun, *J. Am. Chem. Soc.*, 2010, **132**, 1468–1469.

27 Z. Zhu, S. Wang, J. Du, Q. Jin, T. Zhang, F. Cheng and J. Chen, *Nano Lett.*, 2014, **14**, 153–157.

28 P. Zhang, F. Sun, Z. Xiang, Z. Shen, J. Yun and D. Cao, *Energy Environ. Sci.*, 2014, **7**, 442–450.

29 F. Zou, Y. M. Chen, K. Liu, Z. Yu, W. Liang, S. M. Bhaway, M. Gao and Y. Zhu, *ACS Nano*, 2016, **10**, 377–386.

30 L. Shang, H. Yu, X. Huang, T. Bian, R. Shi, Y. Zhao, G. I. Waterhouse, L. Z. Wu, C. H. Tung and T. Zhang, *Adv. Mater.*, 2016, **28**, 1668–1674.

31 H. Li, M. Liang, W. Sun and Y. Wang, *Adv. Funct. Mater.*, 2016, **26**, 1098–1103.

32 L. Zhang, H. B. Wu, S. Madhavi, H. H. Hng and X. W. Lou, *J. Am. Chem. Soc.*, 2012, **134**, 17388–17391.

33 S. J. Yang, S. Nam, T. Kim, J. H. Im, H. Jung, J. H. Kang, S. Wi, B. Park and C. R. Park, *J. Am. Chem. Soc.*, 2013, **135**, 7394–7397.

34 Y. Li, L. Xie, Y. Liu, R. Yang and X. Li, *Inorg. Chem.*, 2008, **47**, 10372–10377.

35 L. Zhou, T. Zhang, Z. Tao and J. Chen, *Nano Res.*, 2014, **7**, 774–781.

36 L. Guo, X. Gu, K. Kang, Y. Wu, J. Cheng, P. Liu, T. Wang and H. Su, *J. Mater. Chem. A*, 2015, **3**, 22807–22815.

37 J. Zhao, F. Cheng, C. Yi, J. Liang, Z. Tao and J. Chen, *J. Mater. Chem.*, 2009, **19**, 4108–4116.

38 M. Kruk and M. Jaroniec, *Chem. Mater.*, 2001, **13**, 3169–3183.

39 J. Liang, Y. Zheng, J. Chen, J. Liu, D. Hulicova-Jurcakova, M. Jaroniec and S. Z. Qiao, *Angew. Chem., Int. Ed.*, 2012, **124**, 3958–3962.

40 S. Yang, X. Feng, X. Wang and K. Müllen, *Angew. Chem., Int. Ed.*, 2011, **50**, 5339–5343.

41 C. Tang, Q. Zhang, M. Q. Zhao, J. Q. Huang, X. B. Cheng, G. L. Tian, H. J. Peng and F. Wei, *Adv. Mater.*, 2014, **26**, 6100–6105.

42 W. H. Shin, H. M. Jung, Y. J. Choi, K. Miyasaka and J. K. Kang, *J. Mater. Chem.*, 2010, **20**, 6544–6549.

43 M. Mahyari and A. Shaabani, *J. Mater. Chem. A*, 2014, **2**, 16652–16659.

44 Y.-Z. Chen, L. Liang, Q. Yang, M. Hong, Q. Xu, S.-H. Yu and H.-L. Jiang, *Mater. Horiz.*, 2015, **2**, 606–612.

45 Y.-Z. Chen, Q. Xu, S.-H. Yu and H.-L. Jiang, *Small*, 2015, **11**, 71–76.